Accurate Segmentation of Arterial Walls in Adaptive Optics Images

Nicolas Lermé, Florence Rossant, Isabelle Bloch, Michel Paques, Edouard Koch

ACCURATE SEGMENTATION OF ARTERIAL WALLS IN ADAPTIVE OPTICS IMAGES

Nicolas Lermé[†] *Florence Rossant*[†] *Isabelle Bloch*[‡] *Michel Pâques*[⋆] *Edouard Koch*[+]

[†] Institut Supérieur d'Électronique de Paris
[‡] Institut Mines-Télécom, Télécom ParisTech, CNRS LTCI
[⋆] CIC 503, Centre Hospitalier National des XX-XV
[+] Centre Hospitalier de Versailles

ABSTRACT

In this paper, a new approach is presented for accurately delineating the artery walls in adaptive optics images. To the best of our knowledge, this is the first paper addressing this problem in this context. To achieve this goal, we propose an automatic two-steps process. The position of inner walls of each vessel is first roughly estimated. Then, a deformable model embedding a parallism constraint is used to refine their positioning and localize the outer walls. Such an approach enables us to model the walls as approximate parallel contours and to control their distance with respect to their common reference line. This model leads to four independent energy functionals, minimized by gradient descent. Noticeably, the evaluation of this new model on healthy subjects shows an overall error smaller than the inter-physicians variability.

***Index Terms*—** Active contours model, adaptive optics, approximate parallelism, retina imaging.

1. INTRODUCTION

Arterial hypertension affects the physiology and structure of small vessels of the retina, which may lead to visual loss. According to the Public Health Agency of Canada, arterial hypertension affects 15 to 20% of the world population. Typically, arterial hypertension results in a thickening of arterial walls, which is predictive of future damage such as stroke [1, 2]. It is therefore of great importance to quantify as accurately as possible the thickness of the arterial wall to document arteriolar damage. But classical fundus photographs cannot capture this level of details due to technological limitations.

Adaptive-Optics (AO) is an opto-electronic technology, first developed in astronomy, which improves the lateral resolution of fundus imaging. AO-based fundus cameras enable the visualization of microstructures such as photoreceptors [3] and capillaries [4]. In the present study, a procedure based on flood-illumination near infrared has been developed [5]. The images acquired with this device have a pixel-resolution of 0.784μm. Blood vessels appear as black elongated structures with a linear axial reflection revealing the center of the vessel. Parietal structures are visible in arterioles as small as 20 microns. The arterial walls appear as a gray line along both sides of the blood column, with a typical thickness equal to about 15% of the lumen (i.e. radius, see Figure 2(a)).

In this paper, we propose an automatic procedure to accurately delineate these walls. To the best of our knowledge, this is the first paper addressing this issue in this context. The following two-steps process is proposed: the position of the inner walls of each vessel is first roughly estimated. Then, a deformable model (Parallel Double Snakes or PDS) embedding a parallelism constraint [6] is used to refine their positioning and localize the outer walls. Such an approach enables us to model the walls as approximate parallel contours and to control their distance with respect to their common reference line. This model leads to four independent energy functionals, minimized by a standard gradient descent method.

The rest of this paper is as follows. In Section 2, we briefly remind a variant of the PDS model with a single almost parallel curve. Then, we detail in Section 3 the two-steps process using this new model and evaluate it in Section 4.

2. PARALLEL DOUBLE SNAKES MODEL

In [6], a parametric active contour model (PDS) has been proposed that simultaneously evolves two curves under a parallelism constraint. In what follows, we propose a variant of this model for extracting a single curve V_1 that is almost parallel to a fixed reference line $V(s) = (x(s), y(s))^T$. Using the same notations, we define the curve

$$V_1(s) = V(s) + b(s)n(s), \tag{1}$$

where n is the normal vector to the curve $V(s)$ and b is the local distance between V and V_1 (see Figure 1). This model allows a direct correspondence between the points of the reference line V and those of the curve V_1. Since the reference line is fixed, the energy of the PDS model reduces to

$$E(V_1, b) = E_{Image}(V_1) + R(V_1, b), \tag{2}$$

Work funded by the ANR project ANR-12-TECS-0015-03 (2013–2015).

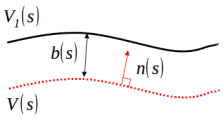

Fig. 1: Parametric representation of a variant of the PDS model.

where the term

$$E_{Image}(V_1) = \int_0^1 P(V_1(s))ds,$$

is designed to attract the curve V_1 towards large intensity gradients in the image I (see [7]). In this context, the term E_{Image} is based on the Gradient Vector Flow (see [8]). The role of the term R in (2) is to control the variation of the distance b, thus imposing a local parallelism. The authors of [6] proposed a function of the derivative of b with

$$R(b) = \int_0^1 Q(s, b')\, ds = \int_0^1 \varphi(s)(b'(s))^2\, ds,$$

where $\varphi(s) \in \mathbb{R}^+$ is an application-dependent parameter (which be tuned later on) that locally controls the strength of the parallelism of the curve V_1 with respect to the reference line V. More precisely, as the parameter $\varphi(s)$ increases, the curve V_1 becomes progressively strictly parallel to the reference line V. Notice that the distance between them has not to be known as prerequisite. It is adjusted during the evolution process and can vary along boundaries. The Euler-Lagrange equation expresses the minimization of (2) w.r.t. $b(s)$

$$\frac{\partial P(V_1(s))}{\partial b} - \frac{d}{ds}\frac{\partial Q(s, b')}{\partial b'} = 0.$$

Finally, the evolution of the distance b is driven by

$$\langle n, -\nabla P(V_1(s))\rangle - 2[\varphi(s)b''(s) + \varphi'(s)b'(s)] = 0. \quad (3)$$

The latter equation is solved by discretizing it and introducing the time variable using standard numerical approximations of derivatives (central difference in space, backward difference in time). The resolution of the above equation stops when the maximum of the absolute difference between two successive estimates of b is smaller than some $\varepsilon \simeq 0$.

3. AUTOMATIC SEGMENTATION OF WALLS

3.1. Pre-segmentation

The source image (see Figure 2(a)) is first enhanced by applying a median filter followed by a non-linear diffusion filter [9]. This filter allows smoothing the blood vessels while preserving the contrast along their edges. The first step of the segmentation is based on the enhancement of the brightest linear structures and the search for the darkest regions, by respectively applying morphological operations and k-means classification ($k = 3$). Both kinds of information are then combined in order to select the linear bright structures corresponding to the vessel axial reflection and compute a binary mask of the vessel (see Figure 2(b)). The vessel is then modeled by the regularized skeleton (denoted by $V(s)$) of its axial reflection [7, 8]. It will serve as reference in all what follows.

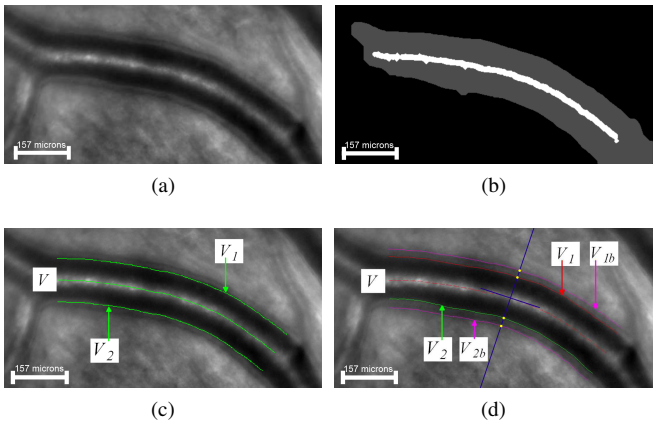

Fig. 2: Segmentation of the parietal structure of a retinal artery: (a) source image; (b) detection of the axial reflection (white) and binary mask of the vessel (light gray); (c) initialization of the active contour model with parallelism constraint (V_1 and V_2 are strictly parallel to V and at equal distance); (d) final segmentation and point correspondence (in yellow) allowing easy and accurate measurements.

The second step of the pre-segmentation process aims at locating the inner borders of the artery. Each border is approximated by a curve parallel to the reference line V (as in (1), with b constant) and is respectively denoted by V_1 and V_2 (see Figure 2(c)). The mean distance b between a side contour and the reference line (i.e. the vessel radius or lumen) is derived from the preprocessed images, by maximizing the mean intensity value of the area delimited by V_1 and V_2 over the mean intensity along them. Dividing by the mean intensity allows pushing these curves towards large image gradients while remaining in dark areas. Thus, these curves are placed as near as possible to the internal side of the parietal structure.

The next step aims at refining the position of V_1, V_2 and at localizing the outer sides of the artery wall, respectively denoted by V_{1b} and V_{2b}.

3.2. Accurate delineation of the walls

Several strategies can be considered to segment arterial walls using the PDS model. A first possible way would consist in using pairwise almost parallel curves with multiple reference lines. Although this model ensures that no crossing occurs between curves, it is computationally heavy to solve and the main reference line is expected to be different from the one found during the pre-segmentation step. To overcome these difficulties, we adopt another (simpler) strategy: use sequen-

tially the variant of the PDS model described in Section 2 (see (3) and (2)). Indeed, the regularized skeleton V of the central reflection marks the centerline of the vessel segment and constitutes a very good reference line, with respect to which we can search for the boundaries of the vessel wall: the inner edges of the arterial walls, V_1 and V_2, on each side of the central reflection V, the outer edges of the arterial walls, V_{1b} and V_{2b}, also on each side of V:

$$\begin{cases} V_1(s) = V(s) + b_1(s)n(s) \\ V_2(s) = V(s) - b_2(s)n(s) \\ V_{1b}(s) = V(s) + b_{1b}(s)n(s) \\ V_{2b}(s) = V(s) - b_{2b}(s)n(s). \end{cases}$$

Although this approach does not ensure no crossing between curves, we never observed such a behavior during experiments. The variant of the PDS model is first applied twice, sequentially, using the pre-segmentation results as initialization ($b_1(s) = b_2(s) = b$, see Figure 2(c)), in order to refine the position of the curves V_1 and V_2 (see Figure 2(d)). So, an accurate localization of the inner edges is obtained. Then, the curve V_1 is translated, by increasing the local radii $b_1(s)$ by a distance d ($b_{1b}(s) = b_1(s) + d$), so that the average gradient along the curve is maximized. This translated curve serves as an initialization for the parallel snake, allowing to get the accurate position of the outer side V_{1b} of the artery wall. The same process is repeated for V_{2b}.

4. EXPERIMENTS AND DISCUSSION

Fourteen images from healthy subjects were manually delineated by three physicians. These physicians have several years of experience in the field of AO image interpretation. The images were selected to ensure the representativeness of the quality and the noise levels encountered by physicians during examinations. The evaluation protocol is as follows: for each selected image, we manually define regularly spaced points on the axial reflection and connect them with a cubic spline [1]. Once regularized by a classical snake as for the pre-segmentation step in Section 3.1, it is then both provided to the automatic procedure and to physicians. Using a common reference line aims at considerably easing the measurements on the arterial walls. Let us now denote by V^M and V^A a manual segmentation and an automatic one, respectively. To compare them, we choose to measure the absolute relative difference of internal and external diameter as well as the walls thickness (i.e. the difference between external and internal diameters), resp. defined for each point by

$$\delta_i(V^M, V^A) = \frac{|d_i(V^M) - d_i(V^A)|}{d_i(V^M)} \times 100, \qquad (4)$$

$$\delta_e(V^M, V^A) = \frac{|d_e(V^M) - d_e(V^A)|}{d_e(V^M)} \times 100, \qquad (5)$$

[1] The robustness of the automatic reference line detection in the pre-segmentation (see Section 3.1) will be evaluated in a forthcoming paper.

$$\delta_w(V^M, V^A) = \frac{|wt(V^M) - wt(V^A)|}{wt(V^M)} \times 100, \qquad (6)$$

where d_e, d_i and wt denote the external diameter, the internal diameter and the walls thickness, respectively. The measure δ_w is of great importance for us. The measures were only taken into account when no bifurcation occurs in vessels (see Figure 3) and when data are available for all physicians. We empirically set $\varphi(s) = 100$ and $\varepsilon = 0.25$ for all the subsequent experiments. Since not enough data were available for measuring the intra-physician variability, we choose the most experienced one as a reference (denoted by Phys_{Ref}). Then, we calculated the inter-physicians variability and the error between the automatic segmentation and the segmentation performed by Phys_{Ref}. The results of this comparison are detailed in Table 1 and illustrated in Figure 3. To put in perspective these results, we also provide between parentheses, the error for which a displacement of one pixel occurs all along a curve. In that case, the numerator of (4), (5) and (6) becomes equal to one. Due the size of arterial walls, we first remark that the error is larger on walls thickness than on internal and external diameters. For 11 images out of 14, the error between our method and the physician reference is smaller than the inter-physicians variability for the walls thickness. For the remaining images, we do believe that this is mainly due to a lack of accuracy in manual segmentations. Due to the poor contrast along walls and the size of these structures, it is indeed difficult for physicians to precisely delineate them (see Subject 6). Also, the computed external wall can be sometimes slightly different from manual segmentations. This can be for instance due to a double contour (see Subject 3). Nevertheless, the overall variability of our method against the physician reference is always lower for all measures. These results therefore validates the proposed approach.

5. REFERENCES

[1] A.M. Heagerty et al., "Small artery structure in hypertension: dual processes of remodeling and growth," *Journal of Hypertension*, vol. 21, pp. 391–397, 1993.

[2] N.H. Buus et al., "Small artery structure during antihypertensive therapy is an independent predictor of cardiovascular events in essential hypertension," *Journal of Hypertension*, vol. 31, no. 4, pp. 791–797, 2013.

[3] J. Liang, D.R. Williams, and D.T. Miller, "Supernormal vision and high-resolution retinal imaging through adaptive optics," *Journal of Optical Society America A*, vol. 14, no. 11, pp. 2884–2892, 1997.

[4] J.A. Martin and A. Roorda, "Direct and noninvasive assessment of parafoveal capillary leukocyte velocity," *Ophthalmology*, vol. 112, no. 12, pp. 2219–2224, 2005.

[5] ImagineEyes, ," http://www.imagine-eyes.com/.

[6] I. Ghorbel, F. Rossant, I. Bloch, and M. Pâques, "Modeling a parallelism constraint in active contours. application to the segmentation of eye vessels and retinal layers," in *Int. Conference on Image Processing*, 2011, pp. 445–448.

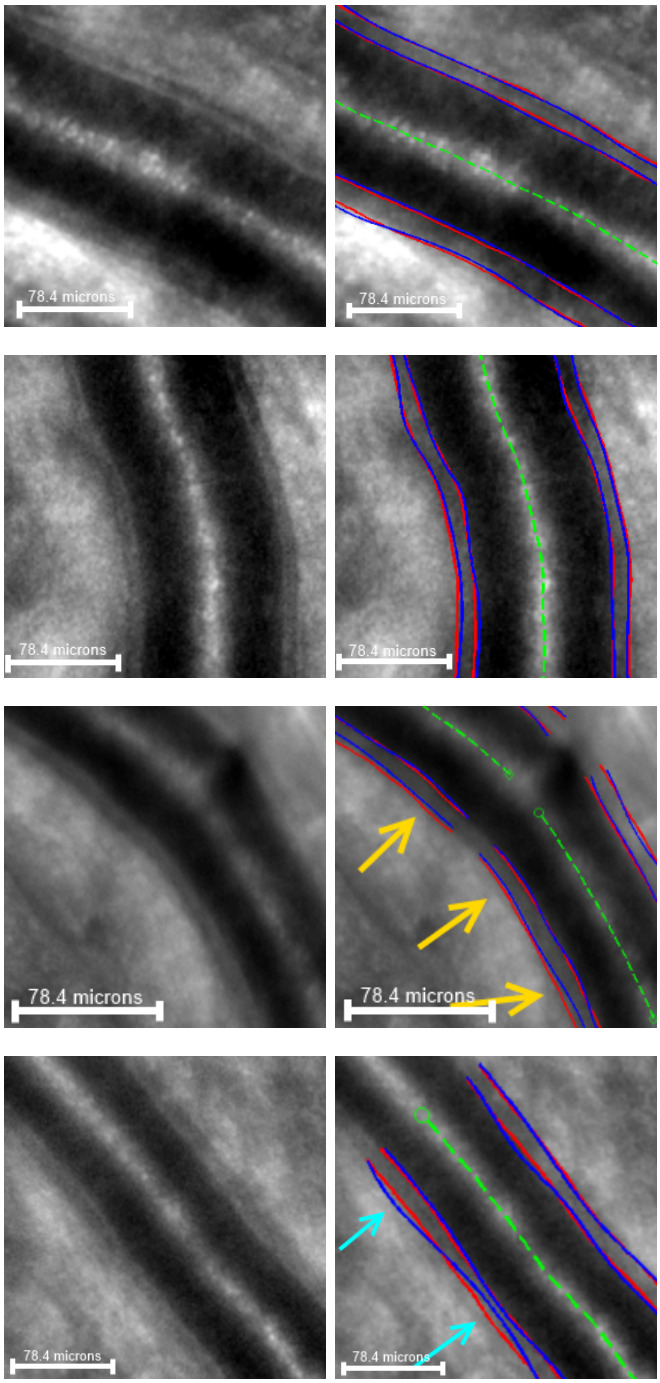

Fig. 3: From top to bottom: positive (half-up) and negative (half-down) results against the reference physician Phys_{Ref} for Subjects 8, 12, 3 and 6 (see Table 1). The manual and the automatic segmentation are drawn in blue and red, respectively. The green dashed line is the reference line. The original images are provided in the left column while they are superimposed to the segmentations in the right column. Yellow and cyan arrows point misplacement of borders in automatic and manual segmentations, respectively.

[7] M. Kass, A. Witkin, and D. Terzopoulos, "Snakes: active contour models," *International Journal of Computer Vision*, vol. 1, no. 4, pp. 321–331, 1988.

[8] C. Xu and J.L. Prince, "Snakes, shapes and gradient vector flow," *IEEE Transactions on Image Processing*, vol. 7, no. 3, pp. 359–369, 1998.

[9] J. Weickert, B.H. Romeny, and M. Viergever, "Efficient and reliable schemes for nonlinear diffusion filtering," *IEEE Transactions on Image Processing*, vol. 7, no. 3, pp. 398–410, 1998.

Subject	Inter-physicians	Our method / Phys_{Ref}
1	2.29 ± 1.54 (1.13 ± 0.04)	1.88 ± 1.08 (1.13 ± 0.04)
2	3.50 ± 2.37 (2.47 ± 0.16)	2.62 ± 1.5 (0.91 ± 0.02)
3	2.86 ± 2.57 (1.37 ± 0.04)	4.41 ± 3.7 (2.47 ± 0.16)
4	2.62 ± 1.93 (2.15 ± 0.08)	1.75 ± 1.21 (1.37 ± 0.04)
5	2.29 ± 1.7 (0.75 ± 0.03)	3.07 ± 2.48 (2.15 ± 0.08)
6	2.79 ± 1.91 (0.89 ± 0.05)	3.3 ± 2.11 (0.89 ± 0.05)
7	3.75 ± 2.8 (1.13 ± 0.05)	2.98 ± 1.64 (0.75 ± 0.03)
8	2.82 ± 2.38 (0.87 ± 0.04)	2.22 ± 2.41 (1.13 ± 0.05)
9	2.84 ± 2.41 (0.97 ± 0.03)	2.44 ± 3.03 (0.87 ± 0.04)
10	3.26 ± 2.65 (0.87 ± 0.03)	3.7 ± 2.94 (0.97 ± 0.03)
11	3 ± 2.08 (0.8 ± 0.02)	4.12 ± 2.47 (0.87 ± 0.03)
12	2.75 ± 1.8 (0.84 ± 0.02)	2.19 ± 2.11 (0.8 ± 0.02)
13	2.7 ± 2.26 (0.9 ± 0.04)	1.65 ± 1.04 (0.84 ± 0.02)
14	3.38 ± 2.27 (0.84 ± 0.05)	1.53 ± 0.97 (0.9 ± 0.04)
Avg	2.91 ± 2.23 (1.04 ± 0.41)	2.68 ± 2.3 (1.04 ± 0.41)

Subject	Inter-physicians	Our method / Phys_{Ref}
1	2.08 ± 1.69 (0.91 ± 0.02)	2.62 ± 1.5 (0.91 ± 0.02)
2	2.2 ± 1.76 (1.7 ± 0.07)	4.14 ± 2.05 (1.7 ± 0.07)
3	2.16 ± 1.53 (1.05 ± 0.03)	5.32 ± 2.39 (1.05 ± 0.03)
4	2.84 ± 2.34 (1.72 ± 0.03)	1.42 ± 1.09 (1.72 ± 0.03)
5	2.8 ± 1.94 (0.6 ± 0.02)	2.37 ± 1.81 (0.6 ± 0.02)
6	2.94 ± 2.19 (0.67 ± 0.03)	2.21 ± 1.52 (0.67 ± 0.03)
7	5.11 ± 3.81 (0.74 ± 0.03)	3.13 ± 1.56 (0.74 ± 0.03)
8	4.05 ± 2.59 (0.65 ± 0.01)	1.98 ± 1.59 (0.65 ± 0.01)
9	1.93 ± 1.36 (0.69 ± 0.02)	2.61 ± 1.14 (0.69 ± 0.02)
10	2.93 ± 1.84 (0.62 ± 0.01)	3.03 ± 1.86 (0.62 ± 0.01)
11	3.03 ± 1.97 (0.6 ± 0.01)	1.84 ± 1.33 (0.6 ± 0.01)
12	2.18 ± 1.95 (0.68 ± 0.01)	2.51 ± 1.27 (0.68 ± 0.01)
13	2.48 ± 1.54 (0.69 ± 0.03)	1.83 ± 1.18 (0.69 ± 0.03)
14	1.7 ± 1.28 (0.68 ± 0.02)	1.47 ± 1.12 (0.68 ± 0.02)
Avg	2.83 ± 2.31 (0.78 ± 0.29)	2.51 ± 1.82 (0.78 ± 0.29)

Subject	Inter-physicians	Our method / Phys_{Ref}
1	10.57 ± 8.1 (4.68 ± 0.59)	10.66 ± 10.57 (4.68 ± 0.59)
2	8.78 ± 6.59 (5.53 ± 0.58)	10.04 ± 6.1 (5.53 ± 0.58)
3	11.63 ± 9.54 (4.63 ± 0.45)	20.88 ± 11.6 (4.63 ± 0.45)
4	17.83 ± 12.89 (8.95 ± 1.61)	16.34 ± 9.65 (8.95 ± 1.61)
5	14.52 ± 11.95 (3.04 ± 0.43)	11.49 ± 7.2 (3.04 ± 0.43)
6	17.46 ± 14.5 (2.8 ± 0.57)	14.48 ± 10.65 (2.8 ± 0.57)
7	14.32 ± 10.93 (2.2 ± 0.29)	11.52 ± 5.86 (2.2 ± 0.29)
8	16.12 ± 10.57 (2.54 ± 0.33)	10.36 ± 9.8 (2.54 ± 0.33)
9	9.85 ± 7.64 (2.46 ± 0.22)	7.32 ± 4.99 (2.46 ± 0.22)
10	14.77 ± 12.36 (2.17 ± 0.32)	12.6 ± 7.26 (2.17 ± 0.32)
11	13.17 ± 8.52 (2.36 ± 0.23)	9.56 ± 6.26 (2.36 ± 0.23)
12	15.98 ± 13.26 (3.67 ± 0.36)	10.29 ± 10.4 (3.67 ± 0.36)
13	12.58 ± 10.11 (2.88 ± 0.22)	7.11 ± 5.55 (2.88 ± 0.22)
14	15.69 ± 10.53 (3.5 ± 0.4)	10.7 ± 8.88 (3.49 ± 0.4)
Avg	14.22 ± 11.42 (3.31 ± 1.48)	11.67 ± 9.13 (3.31 ± 1.48)

Table 1: From top to bottom: inter-physicians and automatic vs reference relative error for internal diameter (see equation (4)), external diameter (see Equation (5)) and walls thickness (see Equation (6)). The numbers between parentheses denote a unit displacement all along the curve (see text).